

# Journal of Mechanics of Materials and Structures

**IMPLEMENTATION OF HAM AND MESHLESS METHOD FOR TORSION OF  
FUNCTIONALLY GRADED ORTHOTROPIC BARS**

Anita Uściłowska and Agnieszka Fraska

**Volume 11, No. 1**

**January 2016**





## IMPLEMENTATION OF HAM AND MESHLESS METHOD FOR TORSION OF FUNCTIONALLY GRADED ORTHOTROPIC BARS

ANITA UŚCIŁOWSKA AND AGNIESZKA FRASKA

The aim of this study is implementation of the Homotopy Analysis Method (HAM) and the Method of Fundamental Solution (MFS) for solving a torsion problem of functionally graded orthotropic bars. The boundary value problem is formulated for the Prandtl's stress function, described by partial differential equation of second order with variable coefficients and appropriate boundary conditions. In the solving process the HAM is used to convert nonlinear equation into a linear one with known fundamental solutions. The Method of Fundamental Solutions supported by Radial Basis Functions and Monomials is suggested for calculate this linear boundary value problem. The numerical experiment has been performed to check the accuracy and the convergence of the presented method.

### 1. Introduction

The torsion problem of bars is an important issue in engineering science. And it is not a new question. Especially twisting of prismatic bars made with homogeneous and isotropic materials have been undertaken by many authors [Kołodziej and Fraska 2005; Nowacki 1970; Naghdi 1994; Timoshenko and Goodier 1970]. In the last time, the case of inhomogeneous and/or anisotropic material is more often discussed in literature [Chen 2011; Horgan and Chan 1998/99; Xu et al. 2010]. It is related to the research on functionally graded materials (FGMs), designed for special engineering applications including aircraft, aerospace, automobile industry and medicine. Functionally graded materials are characterized by the continuous changes of their properties at least in one direction and this feature distinguishes them from the conventional composite materials [Miyamoto et al. 1999]. In fact the concept of FGMs is inspired with materials occurring in nature, such as: bones, skin and bamboo [Jha et al. 2013]. These materials have functionally graded and hierarchical structure and they also have different architecture that results in orthotropic behaviour [Birman and Byrd 2007].

In this work the torsion problem of linear elastic, orthotropic, prismatic bars made with FGMs is investigated. This is a boundary value problem, described by partial differential equation of second order with variable coefficients and appropriate boundary conditions. The problem is formulated for the Prandtl's stress function. Generally, when the shear flexibility moduli are arbitrary functions of cross-sectional coordinates, the analytical solution is not available. In [Ecsedi 2013] non-homogeneous anisotropic (monoclinic) bars were considered, assuming that the shear flexibility moduli are given functions of the Prandtl's stress function of corresponding homogeneous problem. Due this formulation, the obtained analytical solution of the torsion of non-homogeneous monoclinic bar is expressed in terms of the Prandtl's stress functions of a homogeneous monoclinic bar, which has the same cross-section

---

*Keywords:* homotopy analysis method, mesh-free methods, method of fundamental solutions, functionally graded materials, orthotropic symmetry, torsion of a prismatic bar.

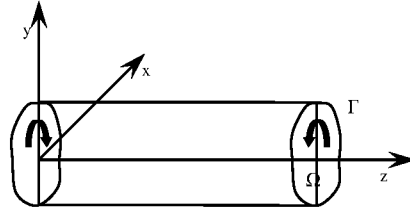


**Figure 1.** Torsion of prismatic bar of arbitrary cross-section  $\Omega$ .

as the non-homogenous bar. But, method proposed by Ecsedi is not universal for any kind of function describing the non-homogeneity of a material. In contrast to Ecsedi's paper, the method presented by us is more general because functions describing the shear flexibility moduli are arbitrary functions of cross-sectional coordinates. We propose the Homotopy Analysis Method combined with the meshless method to solve considered problem. Used mesh-free method is the Method of Fundamental Solutions supported by Radial Basis Functions and Monomials. Uściłowska has examined application of this method in case of isotropic non-homogenous rod [Uściłowska 2010]. The MFS is highly effective method if the fundamental solution of considered equation is available. In the solving process the HAM is used to convert considered equation into a linear one with known fundamental solutions. The HAM was proposed in [Liao 1997]. It is a very useful tool for solving nonlinear problems. Moreover applying HAM with auxiliary parameter  $h$ , allows to control the convergence. Compared with other method often used to adapt MFS to nonlinear problems, based on Picard iteration, it is undoubted advantage of HAM, because in method of Picard iteration the process of iteration may be divergent [Uściłowska 2008].

## 2. Problem description

Consider a functionally graded, orthotropic, linearly elastic bar of an arbitrary and uniform cross-section  $\Omega$ . The axis  $Oz$  is parallel to the longitudinal axis of the bar and the bar is twisted by two couples of forces acting on its ends (see Figure 1). It is assumed that there are no body forces and the bar is free from external forces on its lateral surface. There are no normal stresses on the frontal cross-sections also.

In case of orthotropic bar there are two independent material characteristics  $G_{13}$  and  $G_{23}$  in the torsion equation (see Appendix), where  $G_{13}$  is a shear modulus in direction axis  $x$  on the plane whose is normal in direction  $z$  and adequate  $G_{23}$  is a shear modulus in direction  $y$  on the plane whose is normal in direction  $z$ . We assumed that the shear flexibility moduli  $G_{13}$  and  $G_{23}$ , are the continuous and differentiable functions depending on geometrical coordinates  $x$  and  $y$ .

The problem is formulated in terms of the Prandtl's stress function  $u$  and it is described by the equation [Lekhnitskii 1977]

$$\frac{\partial}{\partial x} \left( \frac{1}{G_{23}(x, y)} \frac{\partial u}{\partial x} \right) + \frac{\partial}{\partial y} \left( \frac{1}{G_{13}(x, y)} \frac{\partial u}{\partial y} \right) = -2 \text{ for } (x, y) \in \Omega, \quad (1)$$

and the boundary condition

$$u = 0 \text{ for } (x, y) \in \Gamma. \quad (2)$$

The stresses are defined as

$$\sigma_{xz} = \theta \frac{\partial u}{\partial y}, \quad \sigma_{yz} = -\theta \frac{\partial u}{\partial x}, \quad (3)$$

where  $\sigma_{xz}$  and  $\sigma_{yz}$  are stress tensor components, and  $\theta$  is the twist angle.

### 3. The numerical algorithm for solving the boundary value problem

The aim of this study is implementation of the Homotopy Analysis Method (HAM) and the Method of Fundamental Solution (MFS) for solving above boundary value problem. For clarity the considered boundary value problem (1)–(2) is rewritten in a general form

$$Au = f \text{ in } \Omega, \quad (4)$$

$$Bu = g \text{ on } \Gamma, \quad (5)$$

where  $A$  is the operator of the partial differential equation (PDE),  $B$  is the operator of the boundary condition,  $u = u(x, y)$  is the unknown function, and  $f, g$  are the given functions on the right hand side of the equations. In considered boundary value problem (BVP)

$$A = \frac{\partial}{\partial x} \left( \frac{1}{G_{23}(x, y)} \frac{\partial}{\partial x} \right) + \frac{\partial}{\partial y} \left( \frac{1}{G_{13}(x, y)} \frac{\partial}{\partial y} \right), \quad B = 1, \quad f = -2 \text{ and } g = 0.$$

In the solution procedure the HAM is applied to convert the considered PDE into a set of linear inhomogeneous equations.

In order to apply the HAM, it is required to construct a linear problem

$$L_g u = L_g u_0 \text{ in } \Omega, \quad (6)$$

$$L_b u = L_b u_0 \text{ on } \Gamma, \quad (7)$$

where  $L_g, L_b$  — are certain linear operators, here  $L_g = \nabla^2, L_b = 1, u_0 = u_0(x, y)$  is the zeroth-order solution.

The proposed homotopy deforms the linear problem (6)–(7) to problem (4)–(5):

$$(1 - \lambda)L_g(U - u_0) = h\lambda(AU - f) \text{ in } \Omega, \quad (8)$$

$$(1 - \lambda)L_b(U - u_0) = h\lambda(BU - g) \text{ on } \Gamma, \quad (9)$$

where  $\lambda$  is the homotopy parameter and  $\lambda \in [0, 1]$ . The additional parameter  $h$  allows controlling the convergence,  $h < 0$ . The solution of the problem is denoted by  $U = U(x, y, \lambda, h)$ . When  $\lambda = 1$  we obtain the equations (4)–(5) and when  $\lambda = 0$  the problem reduces to linear problem (6)–(7) for calculating zeroth-order solution  $u_0 = U(x, y, 0, h)$ .

This homotopy is assumed to be smooth function and the solution of the problem (8)–(9) can be expanded by the Taylor series

$$U(x, y, \lambda, h) = U(x, y, 0, h) + \sum_{i=1}^{\infty} \frac{\lambda^i}{i!} \frac{\partial^i U(x, y, \lambda, h)}{\partial \lambda^i} \Big|_{\lambda=0} = u_0(x, y) + \sum_{i=1}^{\infty} \frac{\lambda^i}{i!} u_0^{(i)}(x, y), \quad (10)$$

where  $u_0^{(i)}(x, y) = \frac{\partial^i U(x, y, \lambda, h)}{\partial \lambda^i} \Big|_{\lambda=0}$ .

Therefore, putting  $\lambda = 1$ , gives us the solution of equations (4)–(5)

$$u(x, y) = U(x, y, 1, h) = u_0(x, y) + \sum_{i=1}^{\infty} \frac{u_0^{(i)}(x, y)}{i!}. \quad (11)$$

Substituting (10) into (8)–(9) and collecting the coefficients of the powers of  $\lambda$  we obtain sequence of linear inhomogeneous PDEs

$$\begin{cases} L_g u_0^{(1)} = h(Au_0 - f) \\ L_g u_0^{(i)} = i(L_g u_0^{(i-1)} + \frac{h}{(i-1)!} \frac{\partial^{i-1}(AU)}{\partial \lambda^{i-1}}|_{\lambda=0}) \end{cases} \text{ for } i = 2, 3, 4, \dots \quad \text{in } \Omega, \quad (12)$$

$$\begin{cases} L_b u_0^{(1)} = h(Bu_0 - g) \\ L_b u_0^{(i)} = 0 \end{cases} \text{ for } i = 2, 3, 4, \dots \quad \text{on } \Gamma. \quad (13)$$

The quantity  $\frac{\partial^{i-1}(AU)}{\partial \lambda^{i-1}}|_{\lambda=0}$  given in formula (12) for operator  $A$  has the following form  $\frac{\partial^{i-1}(AU)}{\partial \lambda^{i-1}}|_{\lambda=0} = A \frac{\partial^{i-1}(U)}{\partial \lambda^{i-1}}|_{\lambda=0} = Au_0^{(i-1)}$ .

The solutions  $u_0^{(i)}(x, y)$  of BVPs (12)–(13) are the elements of the series (10) and (11).

Now each of linear problems (12)–(13) for  $i = 1, 2, 3, \dots$  is solved by means of mesh-free methods that is the MFS supported by approximation by Radial Basis Functions (RBFs).

Let's rewrite the boundary value problem in a general form

$$L_g u_0^{(i)}(x, y) = f^{(i)}(x, y) \text{ in } \Omega, \quad (14)$$

$$L_b u_0^{(i)}(x, y) = g^{(i)}(x, y) \text{ on } \Gamma, \quad (15)$$

where  $f^{(i)}, g^{(i)}$  are the right-hand side functions in (12) and (13), for  $i = 1, 2, 3, \dots$

In the methods of fundamental solutions, the general solution of the  $i$ -th order is decomposed into two parts, a particular solution  $u_p^{(i)}$  and a homogeneous solution  $u_h^{(i)}$

$$u_0^{(i)} = u_p^{(i)} + u_h^{(i)}. \quad (16)$$

The particular solution fulfils (14) but not necessary the boundary condition (15). In order to obtain a particular solution of (14) the right-hand side function  $f^{(i)}$  should be approximated by radial basis function and monomials in the following way:

$$f^{(i)}(x, y, u^{(i-1)}(x, y)) \cong \sum_{k=1}^{N_w} a_k^{(i)} \varphi_k(x, y) + \sum_{l=1}^{N_l} b_l^{(i)} p_l(x, y), \quad (17)$$

where  $\varphi_k(x, y) = \varphi(\|(x - x_k^a, y - y_k^a)\|)$  is RBF, points  $(x_k^a, y_k^a) \in \Omega \cup \Gamma$ , for  $k = 1, 2, \dots, N_w$  are the approximation points placed in considered domain,  $N_w$  is a number of approximation points, and  $p_l(x, y)$  for  $l = 1, 2, \dots, N_l$  are monomials, where  $N_l$  is a number of monomials. As regards coefficients  $a_k^{(i)}$  and  $b_k^{(i)}$ , these are real numbers determined successively in each iteration.

The approximation formula (17) written for each approximation point in the domain, for  $j = 1, \dots, N_w$ , has the form

$$f^{(i)}(x_j^a, y_j^a, u^{(i-1)}(x_j^a, y_j^a)) = \sum_{k=1}^{N_w} a_k^{(i)} \varphi_k(x_j^a, y_j^a) + \sum_{l=1}^{N_l} b_l^{(i)} p_l(x_j^a, y_j^a). \quad (18)$$

Additionally, the condition (19) should be satisfied, to guarantee the limitation of the solution

$$\sum_{k=1}^{N_w} a_k^{(i)} p_l(x_k^a, y_k^a) = 0, \text{ for } l = 1, 2, \dots, N_l. \quad (19)$$

The approximate particular solution of (12) is expressed by the equation

$$u_p^{(i)}(x, y) = \sum_{k=1}^{N_w} a_k^{(i)} \phi_k(x, y) + \sum_{l=1}^{N_l} b_l^{(i)} P_l(x, y), \text{ for } (x, y) \in \Omega. \quad (20)$$

The functions  $\phi_k(x, y)$  and  $P_l(x, y)$  are the particular solutions of the equations

$$L\phi_k(x, y) = \varphi_k(x, y) \text{ for } (x, y) \in \Omega, \quad k = 1, 2, \dots, N_w, \quad (21)$$

$$LP_l(x, y) = p_l(x, y) \text{ for } (x, y) \in \Omega, \quad l = 1, 2, \dots, N_l. \quad (22)$$

In this way the particular solution is obtained. Next stage consists of calculating the homogenous solution on a basis of the dependence

$$u_h^{(i)}(x, y) = \sum_{n=1}^{N_s} c_n^{(i)} f s_n(x, y), \quad (23)$$

where  $f s_n(x, y) = \ln \sqrt{(x - x_n^s)^2 + (y - y_n^s)^2}$  is fundamental solution of the Laplace equation, and  $(x_n^s, y_n^s)$ , for  $n = 1, 2, \dots, N_s$ , are the source points placed outside the region  $\Omega$ ,  $N_s$  is the number of the source points.

By virtue of (16) the coefficients  $c_n^{(i)}$  are calculated from the modified boundary condition

$$\sum_{n=1}^{N_s} c_n^{(i)} f s_n(x_m^b, y_m^b) = -u_p^{(i)}(x_m^b, y_m^b) \text{ for } m = 1, 2, \dots, N_b. \quad (24)$$

The points  $(x_m^b, y_m^b) \in \Gamma$  are the boundary points placed on the contour of the region  $\Omega$ , and  $N_b$  is the number of boundary points.

Finally the general solution of the considered problem is calculated from (11).

The procedure is finished if the parameter defined by formula (25) is a small number, of order  $10^{-5}$

$$d = \|u_0^{(i)}(x, y) - u_0^{(i-1)}(x, y)\| \text{ for } i = 1, 2, \dots \quad (25)$$

At the moment the numerical algorithm for solving the boundary-value problem (12)–(13) is completed.

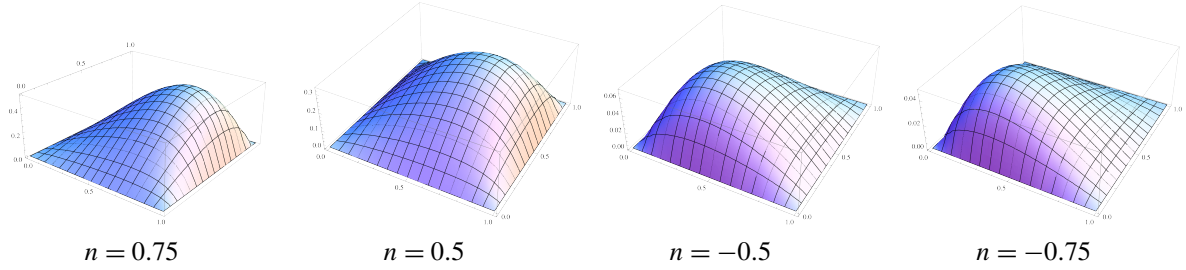


**Figure 2.** Stress function of an FGM orthotropic bar of square cross-section for  $n_1 = n_2 = n$ .

#### 4. Numerical experiment

In order to validating the exactness of the proposed algorithm the numerical experiment has been performed. For the convenient of the computer calculations the non-dimensional variables are introduced as

$$X = \frac{x}{a}, \quad Y = \frac{y}{a}, \quad E = \frac{b}{a}, \quad U(X, Y) = \frac{u(x, y)}{a^2 G_0}, \quad F_1(X, Y) = \frac{G_0}{G_{23}(x, y)}, \quad F_2(X, Y) = \frac{G_0}{G_{13}(x, y)} \quad (26)$$

where  $a, b$  are characteristic geometrical dimensions of the bar's cross-section and the constant  $G_0$  has dimension of the elastic moduli.

The function used during the tests is the thin plate spline RBF described by the formula

$$\varphi_k(X, Y) = (R_k)^2 \ln(R_k), \quad (27)$$

where  $R_k = \sqrt{(X - X_k)^2 + (Y - Y_k)^2}$ .

The others parameters of the MFS are following, the tolerance  $d$  is equal to 0.00001. The boundary points, the approximation points and the source points are distributed uniformly. The source contour is similar to boundary contour and the distance between them  $s$  is 0.2. The number of approximation points  $Nw = 441$ , the number of boundary points  $Nb = 80$ , the number of source points  $Ns = 80$ . The functions describing the inhomogeneity of the material are expressed by the formulas

$$F_1 = e^{-n_1 \pi X}, \quad F_2 = e^{-n_2 \pi Y}. \quad (28)$$

In the example torsion of a bar of a square cross section is considered. The Prandtl stress function in case when  $n_1$  is equal to  $n_2$  is presented in Figure 2. It is easy to observe that the calculated stress function fulfils the boundary condition.

Moreover, if the values of coefficients  $n_1$  and  $n_2$  tend to zero, we approach to homogeneous and isotropic material (see Figure 2). Then analytical solution for the stress function is available and is given by

$$U_a(X, Y) = X(1 - X) - 8 \sum_{k=1,3,\dots}^{\infty} \frac{\sinh(k\pi(1 - Y)) + \sinh(k\pi Y)}{k^3 \pi^3 \sinh(k\pi)} \sin(k\pi X). \quad (29)$$

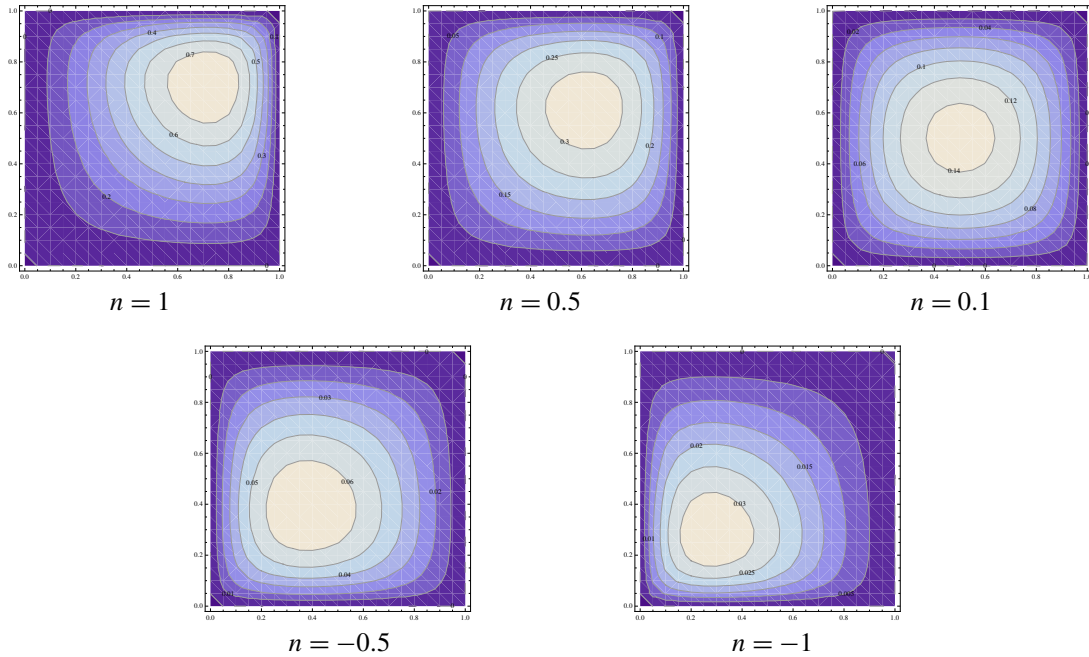


**Figure 3.** Contour map of the stress function of an FGM orthotropic bar of square cross-section for  $n_1 = n_2 = n$ .

Comparison of Figure 3, top right, with Figure 4, left, confirms convergence of results to homogeneous and isotropic case if the coefficients  $n_1$  and  $n_2$  tend to zero. This argues the correctness of the results obtained. The absolute value of the difference between the analytical solution for a homogeneous and isotropic bar and the solution calculated for a orthotropic functionally graded bar in the case  $n_1 = n_2 = 0$  is presented in Figure 4, right. The largest errors, occurring at the corners, are caused of a deficiency in the numerical method. In the method of fundamental solution the maximal errors are localized in corners

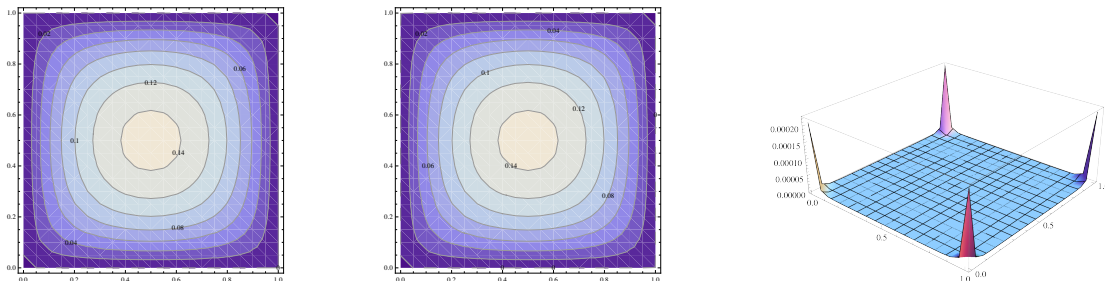


**Figure 4.** Left: Analytical solution for a homogeneous isotropic bar of square cross-section: — the contour map of the stress function. Middle: Contour map of the stress function of an FGM orthotropic bar for  $n_1 = n_2 = 0$ . Right: Plot of the absolute value of the difference between the two solutions.

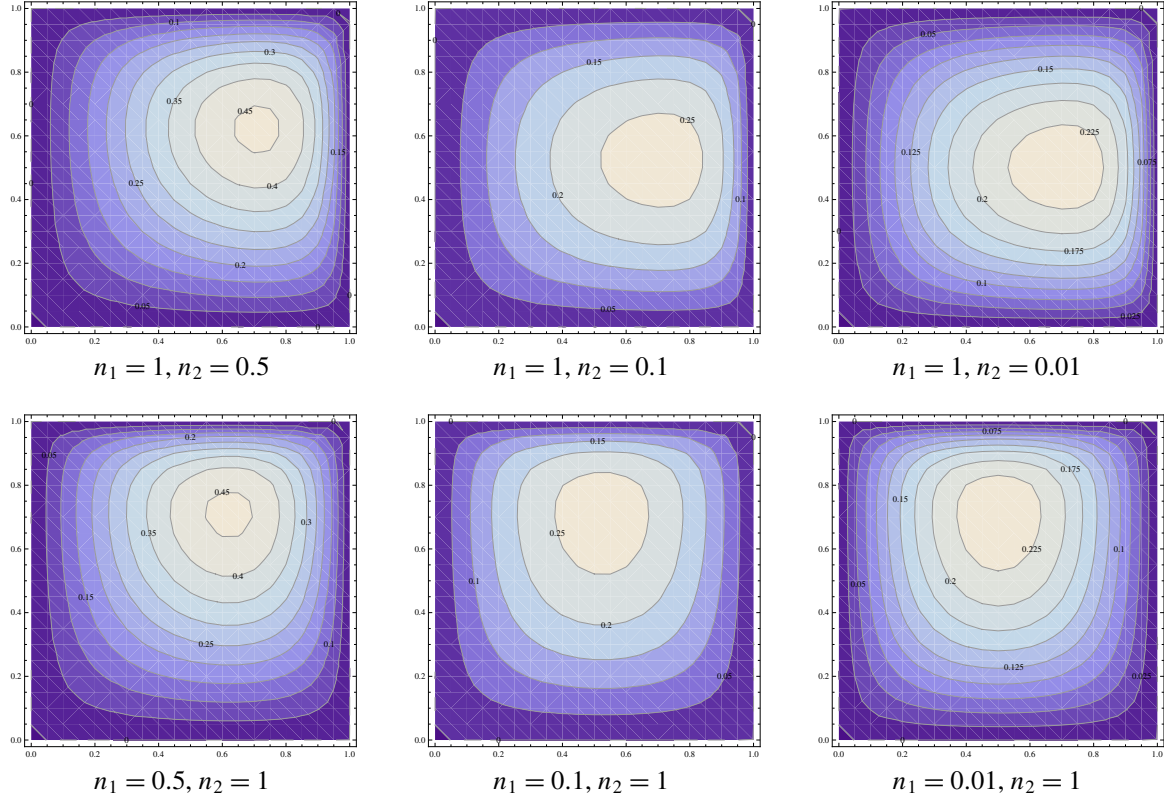


**Figure 5.** Contour map of the stress function of an FGM orthotropic bar of square cross-section.

of the region. Behind the corners, an error of satisfying the boundary conditions is of order  $10^{-5}$ – $10^{-10}$ , and error inside the considered region is oscillated among  $10^{-8}$ – $10^{-9}$ .

Figure 5 shows contour maps of the stress function in case when only one of the coefficients:  $n_1$  or  $n_2$  decreases to zero. This situation refers to functionally graded material with properties of the material changing only in one direction (see the middle and right parts of Figure 5).

Additionally in the method of fundamental solutions obtained approximated solution for the stress function is a continuous function and can be used in the further analysis for instance in stresses calculation. So that on the basis of (3), the resultant of shear stresses is equal to

$$t = \sqrt{t_{xz}^2 + t_{yz}^2}, \quad t_{xz} = \frac{\partial U}{\partial Y}, \quad t_{yz} = -\frac{\partial U}{\partial X}. \quad (30)$$

Here  $t_{xz}$  and  $t_{yz}$  are shear stresses in non-dimensional form, and

$$t_{xz} = \frac{\sigma_{xz}}{a\theta G_0}, \quad t_{yz} = \frac{\sigma_{yz}}{a\theta G_0}. \quad (31)$$

For example the resultant of shear stresses of the investigated rod in case if coefficients  $n_1$  and  $n_2$  equal to each other, are presented in Figure 6. The maximal values of the shear stresses are obtained on the boundary, in the half-length side of the square. It is a result of a class of considered material. If in

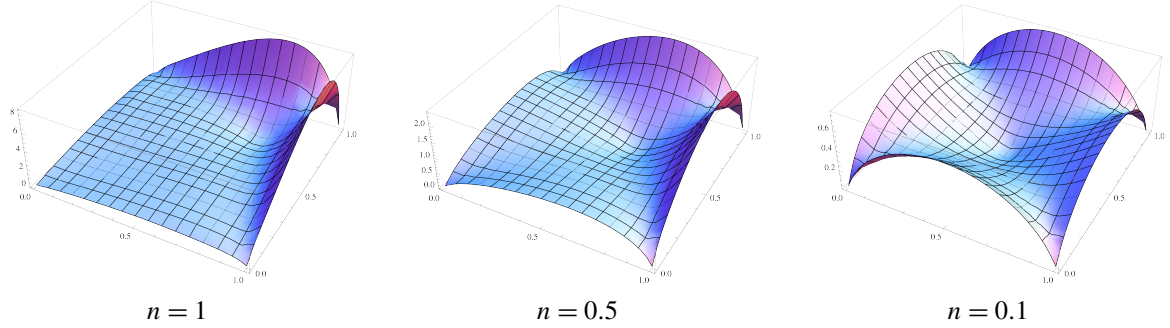


**Figure 6.** Resultant of the shear stresses of an FGM orthotropic bar for  $n_1 = n_2 = n$ .

relations (28) exponents  $n_1$  or/and  $n_2$  tends to zero, functions describing elastic moduli limit to constant values. Therefore the properties of this material reflect the properties of homogeneous one and the maximal stresses occur on the boundary.

The other considered example is done for the orthotropic material defined by the characteristics

$$F_1(X) = G_1 e^{-n\pi X}, \quad F_2(X) = G_2 e^{-n\pi X}, \quad (32)$$

where  $G_1, G_2, n$  are real numbers. The analytical solution is known for the rectangular region of cross-section with the edges length  $X_{\max}, Y_{\max}$  and is given as

$$U_a(X, Y) = \frac{2}{G_1 n \pi} \left( \frac{e^{n\pi/2}}{2 \sinh(n\pi/2)} (e^{n\pi X} - 1) - X e^{n\pi X} \right) - \frac{4}{G_1 \pi^3 (e^{n\pi} - 1)} \sum_{k=1}^{\infty} \frac{e^{n\pi} n^3 \pi + (-1)^k e^{n\pi} (-n^3 \pi + k^2 (-2 + 2e^{n\pi} - n\pi)) + k^2 (2 + e^{n\pi} (-2 + n\pi))}{k(k^2 + n^2)^2} \frac{\sinh(\lambda Y) + \sinh(\lambda(E - Y))}{\sinh(\lambda E)} \sin(k\pi X) \quad (33)$$

where  $\lambda = \pi \sqrt{\frac{G_1}{G_2} (k^2 + n^2/4)}$ ,  $E = Y_{\max}/X_{\max}$ . For the numerical calculation  $X_{\max}$  is taken to be equal to 1.0 and  $G_1 = 1.0$ . The calculations were made for chosen set of values of material characteristics parameters. The maximum relative error, defined as

$$E_{\max} = \max_{\Omega} \left| \frac{U(X, Y) - U_a(X, Y)}{U_a(X, Y)} \right|, \quad (34)$$

where  $\Omega = \{(X, Y) | 0 \leq X \leq X_{\max}, 0 \leq Y \leq Y_{\max}\}$ , is presented in Table 1.

As we can observe the error increases with increase of all pointed parameters. The best result is obtained for the case when material parameters tends to the anisotropic material (the lower error for  $n = 0.1, G_2 = 2$ ). Moreover for all values of  $n$  and  $G_2$  the best results were achieved for square region (see errors for  $Y_{\max} = 1$ ). And the values of the error included in Table 1 are not high and are of the magnitude acceptable for numerical approach. The detailed results are presented on the example of three versions of the geometry parameter and given in Figures 7, 8 and 9.

Figure 7 consists of Prandtl function calculated for  $n = 0.25$  and  $G_2 = 2$ .

$n$	$G_2$	$Y_{\max}$		
		1	2	3
0.1	2	0.036956	0.075664	0.066276
	3	0.047287	0.081257	0.078933
	4	0.054858	0.089432	0.080912
0.25	2	0.063310	0.070291	0.082494
	3	0.082341	0.093817	0.091832
	4	0.106689	0.100982	0.099155
0.5	2	0.066964	0.074529	0.093456
	3	0.081334	0.090123	0.095321
	4	0.091735	0.098231	0.100028

**Table 1.** Maximum relative error for a bar of rectangular cross-section.

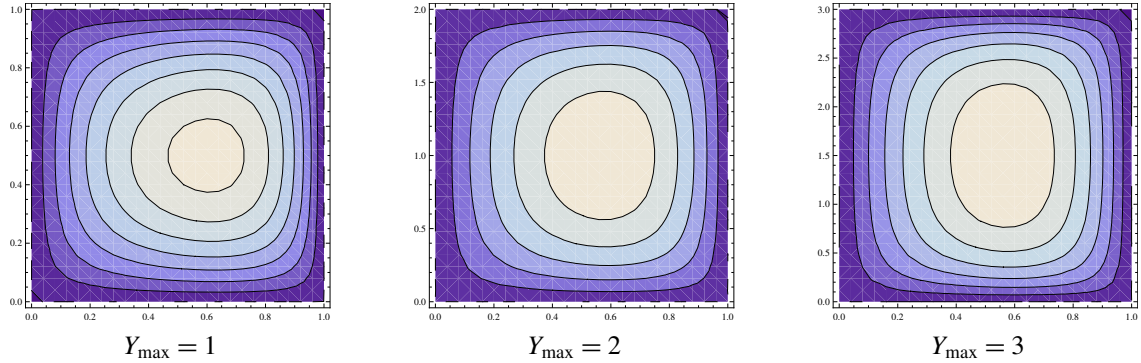


**Figure 7.** The Prandtl function for  $Y_{\max} = 1, 2, 3$ .

The assumption that both material characteristics are functions of one variable —  $X$ , causes the appearance of one symmetry axes of the bar cross-section. The symmetry axes is the line  $Y = Y_{\max}/2$ . Using the symmetry property of Prandtl function and the information about the boundary conditions (2) the maximum values of the Prandtl function may be noticed from Figure 8.

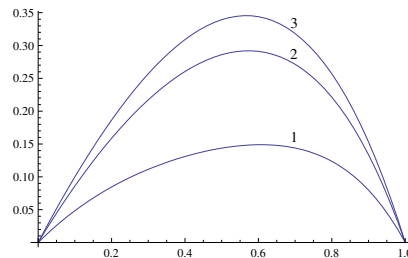


**Figure 8.** Cross-section of the Prandtl function at  $Y = Y_{\max}/2$ , for  $Y_{\max} = 1, 2, 3$ .

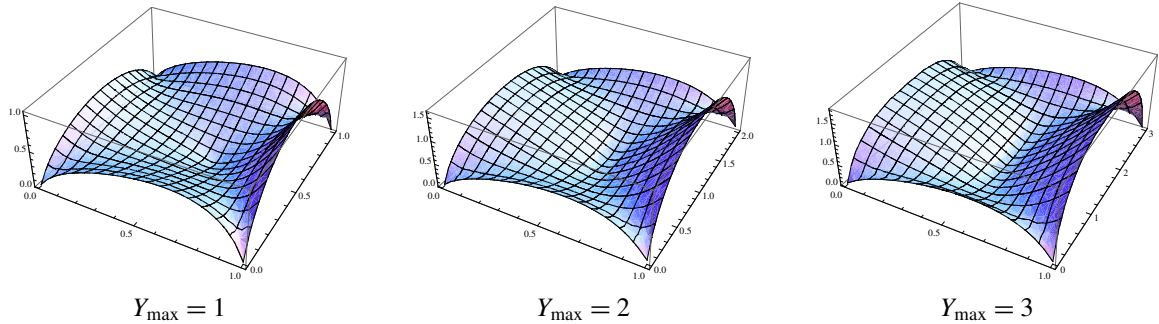


**Figure 9.** Plots of the shear stress for  $Y_{\max} = 1, 2, 3$ .

We can observe that the increase of  $Y_{\max}$  causes the increase of maximum value achieved by Prandtl function. Moreover for larger values of the Prandtl function becomes steeper. Next figure (Figure 9) consists of plots of shear stresses for considered bar with the rectangular cross-section.

The shear stresses get larger for higher values of geometry parameter  $Y_{\max}$ . But for all cases the shear stresses are equal to zero at angles of the bar cross-section. The shear stresses function achieves the local maxima at the middle of each edge of the region  $\Omega$ . Due to symmetry the solutions on the edges  $Y = Y_{\min}$ ,  $Y = Y_{\max}$  are the same, and the maximum value of the shear stress on those edges is the same. On the other pair of edges the shear stress function has different values, so the local maxima are different. One of them (on the edge for  $X = X_{\max}$ ) is the total maximum of the shear stress function.

It is useful to look at the error of the obtained solutions. It is possible to compare the numerically calculated results to the analytical solution (33). The absolute error

$$E_{\text{abs}}(X, Y) = |U(X, Y) - U_a(X, Y)| \quad (35)$$

is plotted on Figure 10. The maximum absolute error appears at point  $(0.8, Y_{\max}/2)$  for  $Y_{\max} = 1$ . The other maximum (local one) is located at  $(0.225, Y_{\max}/2)$ . For the other presented examples four local maxima appear. For  $Y_{\max} = 2$  the local maxima are at points  $(0.24, 0.32)$ ,  $(0.24, 1.68)$ ,  $(0.78, 0.32)$ ,  $(0.78, 1.68)$  and the absolute maximum at points  $(0.24, 0.32)$ ,  $(0.78, 0.32)$  achieves value 0.0072268255. For the case when  $Y_{\max} = 3$  the local maxima are at points  $(0.24, 0.36)$ ,  $(0.24, 2.64)$ ,  $(0.78, 0.36)$ ,  $(0.78, 2.64)$  and the absolute maximum at points  $(0.24, 0.36)$ ,  $(0.78, 0.36)$  achieves value 0.0067483875. The analysing the error plots gives the conclusion that the applied HAM with FSM is a good tool to solve considered problem with demanded accuracy.

The next considered example is the torsion of the bar of elliptic cross-section. The orthotropic material is defined by the characteristics

$$F_1(X) = G_1 e^{-n\pi X}, \quad F_2(X) = G_2 e^{-n\pi Y}. \quad (36)$$

The influence of the characteristics (36) parameters on the shear stress function is investigated.

First, the special case of ellipse is taken into account, i.e. the circle—ellipse with both axes equal to 1.0.

The range of researched  $G_1/G_2$  parameter is  $[1, 3]$ . The Prandtl function and shear stress function are plotted in Figure 11 for  $G_1/G_2 = 2$ .

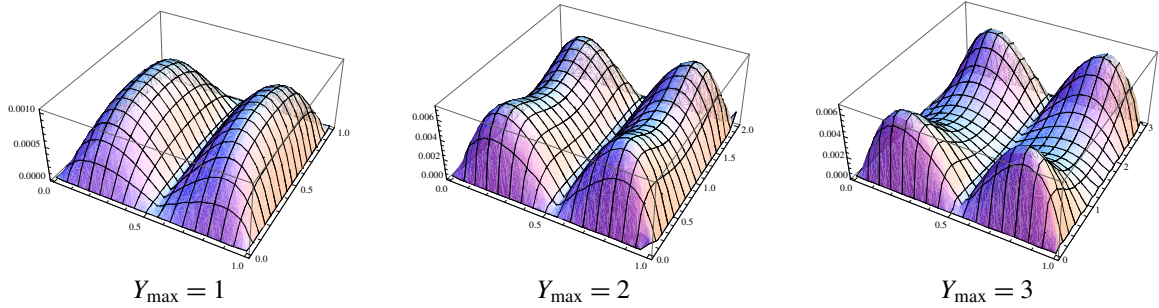


**Figure 10.** Absolute error of the shear stress for  $Y_{\max} = 1, 2, 3$ .

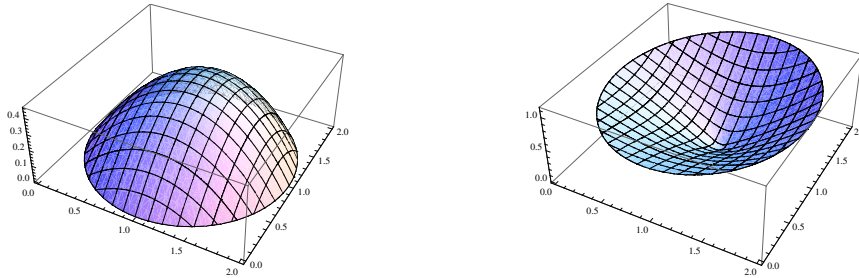


**Figure 11.** Prandtl function (left) and shear stress (right) for a circular cross-section bar with  $G_1/G_2 = 2$ .

	$U_{\max}$	$t_{\max}$	$(X, Y)$ of $t_{\max}$
1	0.6844922646	1.6955413372	(1.7289686274, 1.6845471059)
1.5	0.5475682789	1.3554568654	(1.7289686274, 1.6845471059)
2	0.456262953	1.127726558	(1.5877852523, 1.8090169944)
2.5	0.3910543383	0.9650844154	(1.535826795, 1.8443279255)
3	0.3423152275	0.8432450812	(1.4817536741, 1.87630668)

**Table 2.** Maximum values of the Prandtl function and the shear stress for a circular cross-section bar.

The Prandtl function has one maximum 0.456262953 at point (1.08571, 1.08571). The boundary condition states that the Prandtl function should have value 0.0, and in Figure 11, left, we can see that the boundary condition is fulfilled. Moreover, the shear stress function achieves the minimum value the point (1.08571, 1.08571), which is consistent with physical and mathematical relation of Prandtl and shear stress functions. The maximum value of the shear stress function appears at the boundary, at the point (1.5877852523, 1.8090169944) and has value 1.127726558.

The parameter  $G_1/G_2$  impacts on the maximum value of both the Prandtl function  $U_{\max}$  and shear stress  $t_{\max}$ . In Table 2 the dependence of  $U_{\max}$  and  $t_{\max}$  on parameter  $G_1/G_2$  is shown. For the  $G_1/G_2$  greater than 1.0 the dependence possess the nonlinear decreasing character. The maximum of the Prandtl function appears at the same point. The maximum of the stress function is achieved in different point, but these point is always the boundary point.

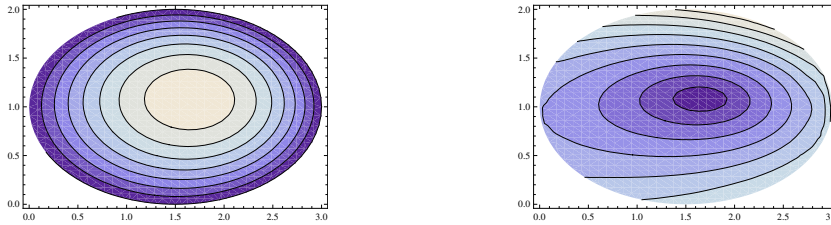


**Figure 12.** Contour maps of the Prandtl function (left) and the shear stress (right) for an elliptic cross-section bar with  $G_1/G_2 = 2$ .

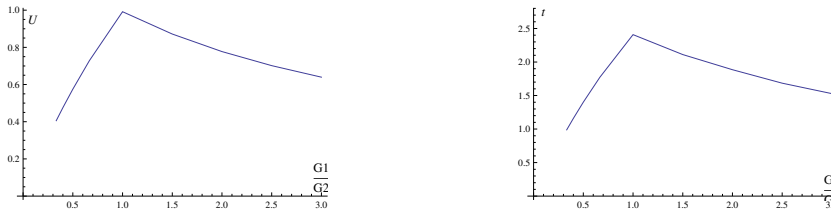


**Figure 13.** Dependence of the Prandtl function (left) and the shear stress (right) of the elliptic cross-section bar on the parameter  $G_1/G_2$ .

In next example we show the influence of material parameters on the stress function appeared in the torsion of the bar with elliptical cross-section. The ratio of ellipse axis is equal to  $3/2$ . The range of researched  $G_1/G_2$  parameter is  $(0, 3]$ . The Prandtl function and the shear stress function are plotted in Figure 12 for  $G_1/G_2 = 2$ . It is more convenient to use contour plots to observe the minima and maxima of these functions. The maximum of the Prandtl function (Figure 12a) has value of 0.575079 and is places at point (1.54286, 1.08571). At the same point the shear stress function (see Figure 12b) achieves the minimum. The maximum of value 1.40104 is achieved by the shear stress function at point (1.75308, 1.98566), which is the boundary point.

The plots given in Figure 13 present the dependence of the maximum values of Prandtl function and the shear stress on the parameter  $G_1/G_2$ . For both functions the dependence has nonlinear character. In the range of  $G_1/G_2$  in  $(0, 1]$  the dependence is increasing function, for  $G_1/G_2$  in  $(1, 3]$  is decreasing one.

We have also consider the bar with cross-section of triangle shape. The triangle has the base of unit length and the subtend angle equal to  $\pi/2$ . The characteristics of the material is given by the formula (36). The top two plots in Figure 14 show the Prandtl and shear stress function for  $G_1/G_2 = \frac{1}{2}$ . We notice that the maximum of the Prandtl function lays on the triangle height perpendicular to the base and has value 0.0198738. The shear stress function has two maxima. They are achieved at the boundary edges, which are not the base. The other situation for the shear stress appears when parameter  $G_1/G_2$  is greater then 1.0. Next we look at the bottom plots in Figure 14, corresponding to  $G_1/G_2 = 2$ . The maximum of the Prandtl function lies on the triangle height perpendicular to the base, as well. But the shear stress function has only one maximum, which lies exactly on the middle of base edge.

In Table 3 the values and coordinates of maxima of the Prandtl and the shear stress functions are presented. The functions of maximum value of Prandtl function and the shear stress with respect to the

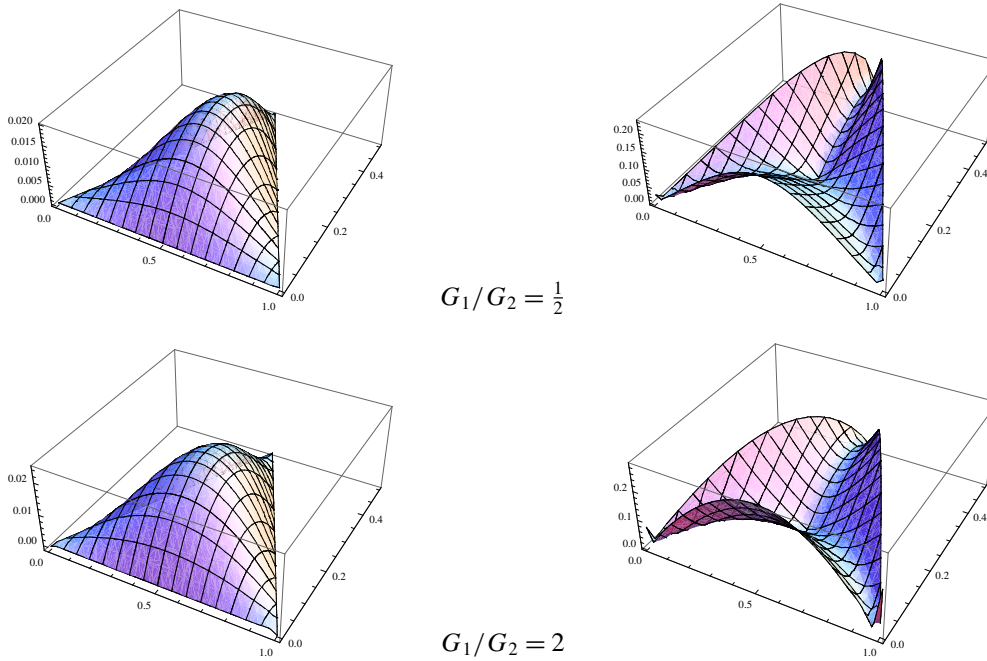


**Figure 14.** Plots of the Prandtl function (left) and the shear stress (right) for a triangular cross-section bar with  $G_1/G_2 = \frac{1}{2}$  (top) and  $G_1/G_2 = 2$  (bottom).

$G_1/G_2$	$U_{\max}$	$(X, Y)$ for $U_{\max}$	$t_{\max}$	$(X, Y)$ for $t_{\max}$
$\frac{1}{3}$	0.0198738	(0.5, 0.216667)	0.230903	(0.63333, 0.366667)
$\frac{2}{3}$	0.0244673	(0.5, 0.215555)	0.280835	(0.6375, 0.3625)
1	0.0322929	(0.5, 0.2)	0.361319	(0.66667, 0.33333)
$\frac{3}{2}$	0.0277619	(0.5, 0.199999)	0.309816	(0.5, 0.)
2	0.0246664	(0.5, 0.183333)	0.289877	(0.5, 0.)

**Table 3.** Values and coordinates of the Prandtl and the shear stress function for a triangular cross-section.

parameter  $G_1/G_2$  are nonlinear and increasing for  $G_1/G_2$  in  $(0, 1]$ , for  $G_1/G_2$  in  $[1, 2]$  these functions become decreasing. The points, at which the maximum of Prandtl function appears, are placed on the triangle height perpendicular to the base and distance between these points and the triangle base decreases with increase of parameter  $G_1/G_2$ . The position of points, at which the shear stress has maximum value, depends on  $G_1/G_2$  in following way. For  $G_1/G_2$  in  $(0, 1]$  there are exists two maxima, at edges which are not base edge. In this case the position of the maximum points is symmetrical, and the height perpendicular to the triangle base is the axis of symmetry. The position of these points changes with the changes of  $G_1/G_2$ . If tends  $G_1/G_2$  to 0.0 the maximum point coordinates tend to the triangle vertex subtend to the base. When  $G_1/G_2$  achieves 1.0 the maximum points are places exactly at the middles of the edges which are not base. When  $G_1/G_2$  is greater than 1.0 the shear stress function has one maximum, which is exactly in the middle of the triangle base.

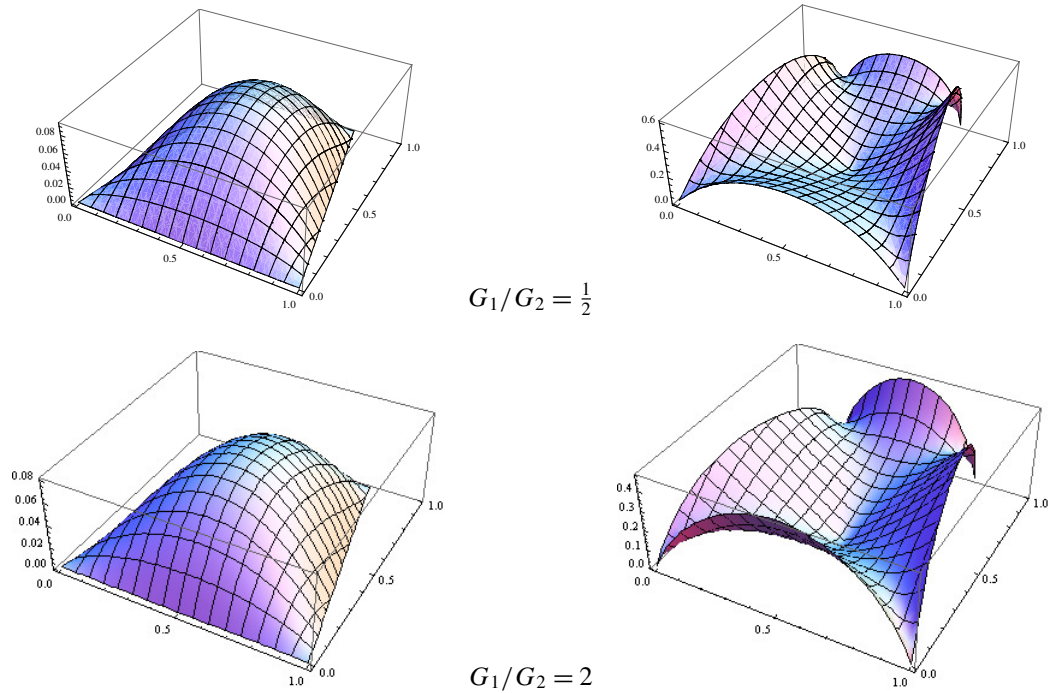


**Figure 15.** Plots of the Prandtl function (left) and the shear stress (right) for a trapezoidal cross-section bar with  $G_1/G_2 = \frac{1}{2}$  (top) and  $G_1/G_2 = 2$  (bottom)

The proposed numerical approach can be used for every shape of the bar cross-section. In this paper the rectangular, elliptic and triangular cross-sections have been tested. The other proposal is to take into account trapezoidal bar. The longer base edge of trapezoid has unit length. The geometrical parameter  $\Delta x$ , which is the half of difference of two parallel edges of the trapezoid, is introduced.

First, the orthotropic material is taken as in formula (36) with  $G_1 = 1$ ,  $G_2 = 2$ ,  $n = 0.1$ . The Prandtl function and the shear stress are shown in the top two plots of Figure 15 for  $\Delta x = 0.2$ . Due to the symmetry of the considered region, the plotted solutions are the symmetric functions, as well. The maximum value of the Prandtl function appears at the point which is placed on the axis of symmetry. The distance of the maximum point from the longer of parallel edges is equal to 0.514286. The maximum value of the shear stress appears on the boundary. The plot presented in Figure 15, top right, shows two maxima (of value 0.603268) on the nonparallel edges of the trapezoid. The other calculations showed that the shear stress function possess two maxima for  $G_1/G_2$  in the range  $(0, 1]$ . When tends  $G_1/G_2$  to 0.0 the position of maximum points tends to the vertex at the shorter of parallel edges. For  $G_1/G_2 = 1$  maxima are placed at the middle of nonparallel edges.

When  $G_1/G_2 = 2$ , the Prandtl function (Figure 15, bottom left) possesses a maximum, located on the symmetry axis at the same distance from the longer of parallel edges as for  $G_1/G_2 = \frac{1}{2}$ . There exists one maximum of the shear stress function (Figure 15, bottom right), placed on the middle of the longer of parallel edges. For the limitary case, when  $\Delta x = 0.0$ , trapezoid becomes square and the second maximum appears on the parallel edge.

As we showed in some numerically solved examples, the proposed numerical algorithm is a good tool for solving the torsion of the bar made of functionally graded materials. In the numerical experiment we performed validation of the solutions using analytical solutions, known for some special cases. And, we showed that the numerical simulations may be done for testing engineering systems, taking into account values of material, geometry and numerical method parameters of certain ranges.

## 5. Conclusions

The homotopy analysis method combined with the meshfree method has been implemented for solving the torsion problem of functionally graded bar with orthotropic symmetry. The numerical experiment has been performed to check the accuracy and the convergence of the proposed method. The advantage of the presented algorithm is easy verification of property calculations, because the precision of the obtained numerical results is confirmed by checking the fulfillment of the boundary conditions. Moreover the obtained solution is a continuous function and can be used in the future analysis for instance in calculation of shear stresses. It is necessary to mention that the functions describing the shear flexibility moduli may be arbitrary functions (continuous and differentiable) of cross-sectional coordinates, and it confirms universality of the proposed method. The further analysis is required for other types of radial basis functions and more complicated shapes of cross-sections or the other classes of FGMs.

## Acknowledgments

This paper was financially supported by Grant 02/21/DSPB/3453 at Poznan University of Technology. The essence of this work was presented during the conference The International Symposium on Trends in Continuum Physics (TRECOP 2014).

## Appendix

The generalized Hooke's law in case of orthotropic symmetry

$$\begin{bmatrix} \epsilon_{xx} \\ \epsilon_{yy} \\ \epsilon_{zz} \\ \epsilon_{yz} \\ \epsilon_{xz} \\ \epsilon_{xy} \end{bmatrix} = \begin{bmatrix} a_{11} & a_{12} & a_{13} & 0 & 0 & 0 \\ a_{12} & a_{22} & a_{23} & 0 & 0 & 0 \\ a_{13} & a_{23} & a_{33} & 0 & 0 & 0 \\ 0 & 0 & 0 & a_{44} & 0 & 0 \\ 0 & 0 & 0 & 0 & a_{55} & 0 \\ 0 & 0 & 0 & 0 & 0 & a_{66} \end{bmatrix} \begin{bmatrix} \sigma_{xx} \\ \sigma_{yy} \\ \sigma_{zz} \\ \sigma_{yz} \\ \sigma_{xz} \\ \sigma_{xy} \end{bmatrix} \quad (\text{A.1})$$

where the elements of the compliance matrix  $a_{ij}$  are given in terms of engineering properties by

$$\begin{bmatrix} \epsilon_{xx} \\ \epsilon_{yy} \\ \epsilon_{zz} \\ \epsilon_{yz} \\ \epsilon_{xz} \\ \epsilon_{xy} \end{bmatrix} = \begin{bmatrix} 1/E_1 & \nu_{12}/E_2 & \nu_{13}/E_3 & 0 & 0 & 0 \\ \nu_{12}/E_2 & 1/E_2 & \nu_{23}/E_3 & 0 & 0 & 0 \\ \nu_{13}/E_3 & \nu_{23}/E_3 & 1/E_3 & 0 & 0 & 0 \\ 0 & 0 & 0 & 1/G_{23} & 0 & 0 \\ 0 & 0 & 0 & 0 & 1/G_{13} & 0 \\ 0 & 0 & 0 & 0 & 0 & 1/G_{12} \end{bmatrix} \begin{bmatrix} \sigma_{xx} \\ \sigma_{yy} \\ \sigma_{zz} \\ \sigma_{yz} \\ \sigma_{xz} \\ \sigma_{xy} \end{bmatrix} \quad (\text{A.2})$$

$E_1, E_2, E_3$  — Young moduli,  $\nu_{12}, \nu_{13}, \nu_{23}$  — Poisson ratios,  $G_{12}, G_{13}, G_{23}$  — shear moduli.

## References

- [Birman and Byrd 2007] V. Birman and L. W. Byrd, “Modeling and analysis of functionally graded materials and structures”, *Applied Mechanics Reviews* **60**:5 (09/01 2007), 195–216.
- [Chen 2011] T. Chen, “A novel class of graded cylinders neutral to host shafts of arbitrary cross-sections under torsion”, *Mechanics Research Communications* **38**:1 (2011), 68–71.
- [Ecsedi 2013] I. Ecsedi, “Some analytical solutions for Saint-Venant torsion of non-homogeneous anisotropic cylindrical bars”, *Mechanics Research Communications* **52** (2013), 95–100.
- [Horgan and Chan 1998/99] C. O. Horgan and A. M. Chan, “Torsion of functionally graded isotropic linearly elastic bars”, *J. Elasticity* **52**:2 (1998/99), 181–199.
- [Jha et al. 2013] D. K. Jha, T. Kant, and R. K. Singh, “A critical review of recent research on functionally graded plates”, *Composite Structures* **96** (2013), 833–849.
- [Kołodziej and Fraska 2005] J. A. Kołodziej and A. Fraska, “Elastic torsion of bars possessing regular polygon in cross-section using BCM”, *Computers & Structures* **84**:1–2 (2005), 78–91.
- [Lekhnitskii 1977] S. G. Lekhnitskii, Теория упругости анизотропного тела, 2nd ed., Nauka, Moscow, 1977. Translated as *Theory of elasticity of an anisotropic body*, Mir, Moscow, 1981.
- [Liao 1997] S.-J. Liao, “Homotopy analysis method: a new analytical technique for nonlinear problems”, *Communications in Nonlinear Science and Numerical Simulation* **2**:2 (1997), 95–100.
- [Miyamoto et al. 1999] Y. Miyamoto, W. A. Kaysser, B. H. Rabin, A. Kawasaki, and R. G. Ford (editors), *Functionally graded materials: design, processing and applications*, Materials Technology Series **5**, Springer, New York, 1999.
- [Naghdi 1994] A. K. Naghdi, “Torsion of rectangular bars with multiple cylindrical reinforcement or cavities”, *Journal of Applied Mechanics* **61**:2 (06/01 1994), 483–487.
- [Nowacki 1970] W. Nowacki, *Teoria sprężystości*, Państwowe Wydawnictwo Naukowe, Warszawa, 1970.
- [Timoshenko and Goodier 1970] S. P. Timoshenko and J. N. Goodier, *Theory of elasticity*, 3rd ed., McGraw-Hill, New York, 1970.
- [Uściłowska 2008] A. Uściłowska, *Rozwiązywanie wybranych zagadnień nieliniowych mechaniki metodą rozwiązań podstawowych*, Wydawnictwo Politechniki Poznańskiej, Poznań, 2008.
- [Uściłowska 2010] A. Uściłowska, “Implementation of the method of fundamental solutions and homotopy analysis method for solving a torsion problem of a rod made of functionally graded material”, *Advanced Materials Research* **123–125** (Aug 2010), 551–554.
- [Xu et al. 2010] R. Xu, J. He, and W. Chen, “Saint-Venant torsion of orthotropic bars with inhomogeneous rectangular cross section”, *Composite Structures* **92**:6 (2010), 1449–1457.

Received 20 Dec 2014. Revised 27 Aug 2015. Accepted 11 Oct 2015.

ANITA UŚCIŁOWSKA: [anita.uscilowska@put.poznan.pl](mailto:anita.uscilowska@put.poznan.pl)

*Institute of Materials Technology, Poznan University of Technology, ul. Piotrowo 3, 60-965 Poznań, Poland*

AGNIESZKA FRASKA: [agnieszka.fraska@put.poznan.pl](mailto:agnieszka.fraska@put.poznan.pl)

*Institute of Applied Mechanics, Poznan University of Technology, ul. Jana Pawła II 24, 60-695 Poznań, Poland*



# JOURNAL OF MECHANICS OF MATERIALS AND STRUCTURES

[msp.org/jomms](http://msp.org/jomms)

Founded by Charles R. Steele and Marie-Louise Steele

## EDITORIAL BOARD

ADAIR R. AGUIAR University of São Paulo at São Carlos, Brazil  
KATIA BERTOLDI Harvard University, USA  
DAVIDE BIGONI University of Trento, Italy  
YIBIN FU Keele University, UK  
IWONA JASIUK University of Illinois at Urbana-Champaign, USA  
C. W. LIM City University of Hong Kong  
THOMAS J. PENCE Michigan State University, USA  
DAVID STEIGMANN University of California at Berkeley, USA

## ADVISORY BOARD

J. P. CARTER University of Sydney, Australia  
D. H. HODGES Georgia Institute of Technology, USA  
J. HUTCHINSON Harvard University, USA  
D. PAMPLONA Universidade Católica do Rio de Janeiro, Brazil  
M. B. RUBIN Technion, Haifa, Israel

**PRODUCTION** [production@msp.org](mailto:production@msp.org)

SILVIO LEVY Scientific Editor

Cover photo: Ev Shafir

---

See [msp.org/jomms](http://msp.org/jomms) for submission guidelines.

---

JoMMS (ISSN 1559-3959) at Mathematical Sciences Publishers, 798 Evans Hall #6840, c/o University of California, Berkeley, CA 94720-3840, is published in 10 issues a year. The subscription price for 2016 is US\$575/year for the electronic version, and \$735/year (+\$60, if shipping outside the US) for print and electronic. Subscriptions, requests for back issues, and changes of address should be sent to MSP.

---

JoMMS peer-review and production is managed by EditFLOW<sup>®</sup> from Mathematical Sciences Publishers.

PUBLISHED BY

 **mathematical sciences publishers**  
**nonprofit scientific publishing**

<http://msp.org/>

© 2016 Mathematical Sciences Publishers

## Special issue

### Trends in Continuum Physics (TRECOP 2014)

Preface	BOGDAN T. MARUSZEWSKI, WOLFGANG MUSCHIK, ANDRZEJ RADOWICZ and KRZYSZTOF W. WOJCIECHOWSKI	1
Stress and displacement analysis of an auxetic quarter-plane under a concentrated force	PAWEŁ FRITZKOWSKI and HENRYK KAMIŃSKI	3
Laminar flow of a power-law fluid between corrugated plates	JAKUB KRZYSZTOF GRABSKI and JAN ADAM KOŁODZIEJ	23
A study of elastic-plastic deformation in the plate with the incremental theory and the meshless methods	MALGORZATA A. JANKOWSKA and JAN ADAM KOŁODZIEJ	41
Implementation of HAM and meshless method for torsion of functionally graded orthotropic bars	ANITA UŚCIEŁOWSKA and AGNIESZKA FRASKA	61
The application of the method of fundamental solutions in modeling auxetic materials	TOMASZ WALCZAK, GRAZYNA SYPNIEWSKA-KAMIŃSKA, BOGDAN T. MARUSZEWSKI and KRZYSZTOF W. WOJCIECHOWSKI	79

